Ion-Ripple Laser

K. R. Chen and J. M. Dawson

Department of Physics, University of California at Los Angeles, Los Angeles, California 90024

(Received 11 March 1991; revised manuscript received 1 July 1991)

We present a new scheme, the ion-ripple laser, for generating tunable coherent radiation ranging from microwaves to the ultraviolet. A relativistic electron beam obliquely propagating through an ion ripple excites electromagnetic radiation which is coupled to a negative-energy electrostatic wave via backward Raman scattering. The radiation peaks at a resonance frequency of $\omega \sim 2\gamma^2 k_{ir} c \cos\theta$. We derive the fluid theory dispersion relation for wave coupling and estimate the nonlinear saturation level. A 1 2/2 D PIC simulation code is used to verify the theory and scaling laws.

PACS numbers: 42.55.Tb, 52.35.Fp, 52.40.Mj, 52.65.+z

We develop here a new scheme to generate tunable coherent radiation. The basic concept is the use of a relativistic electron beam obliquely propagating through an ion ripple, as shown in Fig. 1. This mechanism may be capable of producing radiation from microwaves to the ultraviolet. Electromagnetic radiation results from backward Raman scattering with a peak growth rate at a resonance frequency $\omega \sim 2\gamma^2 k_{ir} c \cos\theta$, where γ is the beam's Lorentz factor, c is the speed of light, k_{ir} is the wave number of the ion ripple, and θ is the angle between the beam and the ripple.

The first step is to create a plasma density variation or ripple. For example, a sound wave can be used to modulate the density of a neutral gas which is then ionized by a laser pulse [1]. Another way is to excite an ion acoustic wave in a neutral plasma. The wave number of the plasma ripple is equal to that of the ion acoustic wave, $k_{ir} = \omega_{ir}/c_s$, where ω_{ir} is the frequency of the ion acoustic wave, and c_s is the ion acoustic speed.

In order to produce radiation from the neutral plasma ripple, a relativistic electron beam is injected into the plasma ripple at an angle θ. As long as the beam density n_b is equal to or higher than the plasma density n_0, the plasma electrons will be expelled from the path of beam [2] in response to the space charge of the beam electrons. The ion ripple will then be seen as a stationary undulator force by the beam electrons.

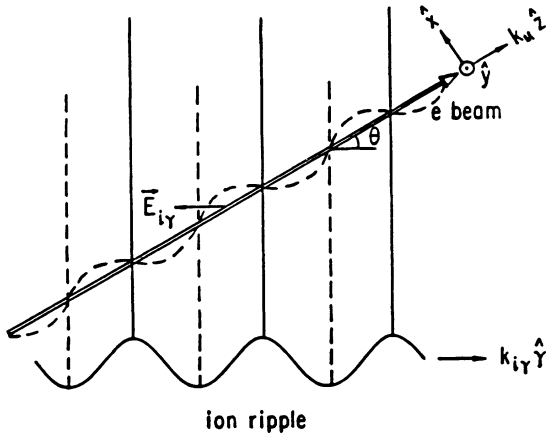

FIG. 1. A relativistic electron beam propagates through an ion ripple with an angle θ. The dashed curve is the actual beam trajectory, while the straight arrow is the original beam path.

We take the density of the ion ripple to be $n_i = n_0[1 + \epsilon_{ir} \sin(k_{ir} r)]$, where ϵ_{ir} is the perturbation ripple density, and $\hat{\mathbf{r}}$ is the ripple direction. Since the beam velocity v_0 is much greater than the acoustic velocity c_s, the ion ripple can be treated as stationary. If the transverse, $(\hat{\mathbf{x}}, \hat{\mathbf{y}})$, variation of the ion ripple field on the beam electron is negligible, as shown in Fig. 1, the spatial variation can be simplified to one dimension. The electric field seen by the beam can be expressed by

$$\mathbf{E}_{ir} = \frac{4\pi n_0 e}{k_u} \epsilon_i \cos(k_u z)[\hat{\mathbf{x}} \sin\theta - \hat{\mathbf{z}} \cos\theta] , \tag{1}$$

where $\epsilon_i = \epsilon_{ir} \cos\theta$ is the fractional ripple of ion density, and $k_u = k_{ir} \cos\theta$. The longitudinal $(\hat{\mathbf{z}})$ part of $\mathbf{E}_{ir}$ may excite electrostatic instabilities [3]; this becomes unimportant if $k_u c \gg \omega_{pe}/\gamma^{3/2}$, where $\omega_{pe}^2 = 4\pi n_0 e^2/m_e$ is the plasma frequency and m_e is the rest mass of the electron. Subjected to the transverse $(\hat{\mathbf{x}})$ field of $\mathbf{E}_{ir}$, the beam electrons execute transverse oscillations, which are the source of the energy needed to produce the electromagnetic radiation [4].

We will first derive the dispersion relation from fluid theory [5] in order to study the growth rate and spectrum of the radiation. The nonlinear saturation level is estimated from the trapping of beam electrons by the electrostatic potential wells of the beam mode. The effects of energy spread and emittance are discussed. We also use a 1 2/2 D (1D in space, 3D in momenta and fields) electromagnetic particle-in-cell (PIC) simulation code [6] to check the validity of the analytic theory, and to study the nonlinear effects. Comparison with conventional free-electron lasers (FELs) [4,5,7,8] is also provided.

The equations needed to derive the dispersion relation are Maxwell equations, the continuity equation, and the

equation of electron motion, and are given by

$$\nabla_z \cdot E_z = 4\pi(n_i - n_b)e ,$$

$$\nabla_z \times E_x = -\frac{1}{c}\frac{\partial B_y}{\partial t} ,$$

$$\nabla_z \times B_y = \frac{4\pi}{c} j_x + \frac{1}{c}\frac{\partial E_x}{\partial t} , \tag{2}$$

$$0 = \frac{\partial n_b}{\partial t} + \frac{P_z}{\gamma m_e}\frac{\partial n_b}{\partial z} + \frac{n_b}{m_e}\frac{\partial}{\partial z}\left(\frac{P_z}{\gamma}\right) ,$$

$$\frac{d\mathbf{P}}{dt} = -e\left(\mathbf{E} + \frac{\mathbf{P}\times\mathbf{B}}{\gamma m_e c}\right) - \frac{3\kappa T}{n_b}\frac{\partial n_b}{\partial z}\hat{\mathbf{z}} ,$$

where E_x, E_z, and $\mathbf{E}$ are the electric fields, B_y and $\mathbf{B}$ are the magnetic fields, $j_x = -n_b e v_x$ is the transverse current of beam electrons, P_x, P_z, and $\mathbf{P}$ are the momenta of the beam electron, κT is the beam electron temperature and is assumed small, and the beam density is assumed, on average, to be the same as the plasma (ion) density.

For $\epsilon_i \ll 1$ and a small amplitude electromagnetic wave ($E_1 \ll |\mathbf{E}_{ir}|$), we obtain the dispersion relation

$$\varepsilon_{em}\varepsilon_{es} = C_f , \tag{3}$$

where

$$\varepsilon_{em} = \omega^2 - k^2c^2 - \omega_{pe}^2/\gamma ,$$

$$\varepsilon_{es} = (\omega - k_p v_0)^2 - \frac{\omega_{pe}^2 + 3k_p^2 v_{tz}^2}{\gamma^3} ,$$

$C_f = k^2 v_0^2 \beta_u^2 \omega_{pe}^2/4\gamma^3$, for $\gamma \gg 1$, is the coupling factor of the electromagnetic (EM) mode and the electrostatic mode through the ion-ripple pump mode,

$$\beta_u = -\epsilon_i \sin\theta\,(\omega_{pe}^2/\gamma)/(\beta_0^2\omega_{pe}^2/\gamma + k_u^2 v_0^2) ,$$

$\beta_0 = v_0/c$, v_{tz} is the electron thermal velocity, and $\varepsilon_{em} = 0$ is the dispersion relation of an electromagnetic mode with a wave number k in a uniform plasma, while $\varepsilon_{es} = 0$ is the dispersion relation for an electrostatic mode with a wave number $k_p = k + k_u$ (the conservation of momentum) in a uniform plasma. The wave frequency can be determined by the intersection of their dispersion curves; that is, $\omega_{em} = \omega_{es}$ (the conservation of energy), where $\omega_{em} = (k^2c^2 + \omega_{pe}^2/\gamma)^{1/2}$ is the frequency of the EM mode, $\omega_{es} = k_p v_0 - S$ is the frequency of slow electrostatic beam mode, and $S = (\omega_{pe}^2 + 3k_p^2 v_{tz}^2)^{1/2}/\gamma^{3/2}$. Thus, for $\gamma \gg 1$, the wave number of the backward Raman scattered EM mode is $k \sim 2\gamma^2(k_{ir} v_0 \cos\theta - S)/c$. This reveals the scaling of the radiation frequency including Doppler shifts and space-charge effects. The reason we use the term "backward" is that, in the beam frame, the undulator field acts like an incoming wave and the radiation is in the opposite direction.

By solving Eq. (3), we obtain the radiation frequency $\omega = \omega_r + i\omega_i$; $\omega_r = \omega_{em} - \Delta/2$ and $\omega_i = (-\Delta^2 + C_f/S\omega_{em})^{1/2}/2$, where $\Delta = \omega_{em} - \omega_{es}$ and $\delta = \omega_r - \omega_{es} = \Delta/2$ is the mismatch factor [4]. Resonance occurs at $\delta \sim 0$ so that the requirement for instability is $C_f S > 0$. The spectrum can be estimated by the coupling factor $C_f > S\omega_{em}\Delta^2$ (mismatch). The maximum growth rate is $\omega_i = \omega_{pe}^{5/2}\epsilon_i \sin\theta/\gamma^{3/4}(2k_u c)^{3/2}$. The nonlinear saturation mechanism of the ion-ripple laser (IRL) is expected to be due to beam electrons being trapped by the electrostatic potential wells. Then the efficiency of a cold beam may be estimated to be $\eta = (\gamma - \gamma_{ph})/(\gamma - 1)$, where $\gamma_{ph} = (1 - v_{ph}^2/c^2)^{-1/2}$, and $v_{ph} = v_0 - S/k_p$ is the phase velocity of the slow electrostatic beam mode. The efficiency $\eta = \omega_{pe}/2k_u c\gamma^{3/2}$. The cold beam limit is valid only if [9] $v_s' < |v_{ph}'|$, where v_s' is the velocity spread, and the superscript denotes the quantities in the beam frame. In the laboratory frame, for $\gamma \gg 1$, the condition becomes $\Delta\gamma/\gamma < \eta$, where $\Delta\gamma$ is the axial energy spread. The normalized beam emittance ϵ_n gives an effective $\Delta\gamma$; that is, $\Delta\gamma/\gamma \sim (\epsilon_n/a)^2/2$, where a is the radial size of a cylindrical beam.

We checked the validity of the above theory by a 1 2/2 D PIC simulation code which begins with the equilibrium state plus a small amount of random thermal noise to start the growth. Figure 2 shows the growth rate of an EM wave for the case of $\gamma = 3$, $k_u c = 1.6\omega_{pe}$, $\theta = 45°$, and $\epsilon_i = 0.3$ and $\epsilon_i = 0.2$, respectively. The simulations agree well with the theory and verify that increasing ϵ_i (i.e., increasing C_f) makes the growth rate larger and the spectrum broader. From simulation, we know $k_p = k + k_u$ and $\omega_{em} \sim \omega_{es}$ are satisfied (not shown). Hence, the instability is due to backward Raman scattering.

The time evolution of the radiation wave energy (Fig. 3) gives the efficiency $\eta \sim 7\%$, while the theoretical esti-

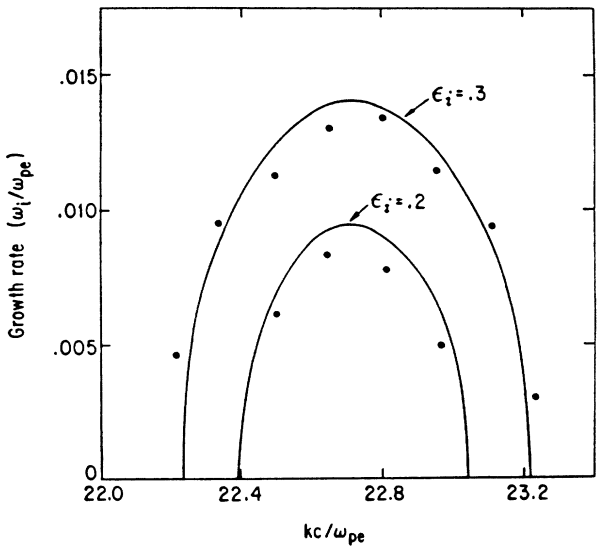

FIG. 2. Growth rate from theory (solid lines) and simulation (discrete points) vs wave number for the cases of $\gamma = 3$, $\theta = 45°$, $k_u c/\omega_{pe} = 1.6$, and $\epsilon_i = 0.2$ and $\epsilon_i = 0.3$, respectively.

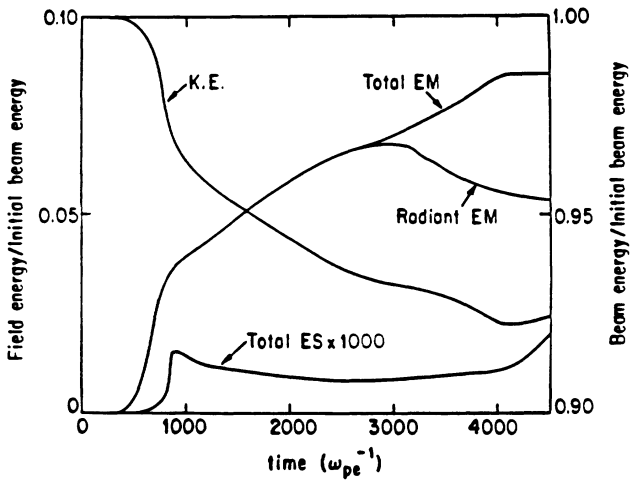

FIG. 3. Time evolution of beam kinetic, total electrostatic, total electromagnetic, and radiant electromagnetic wave energy for the case of $\gamma=3$, $\theta=45°$, $k_u c/\omega_{pe}=1.6$, and $\epsilon_i=0.3$. The electrostatic energy is multiplied by a factor of 1000.

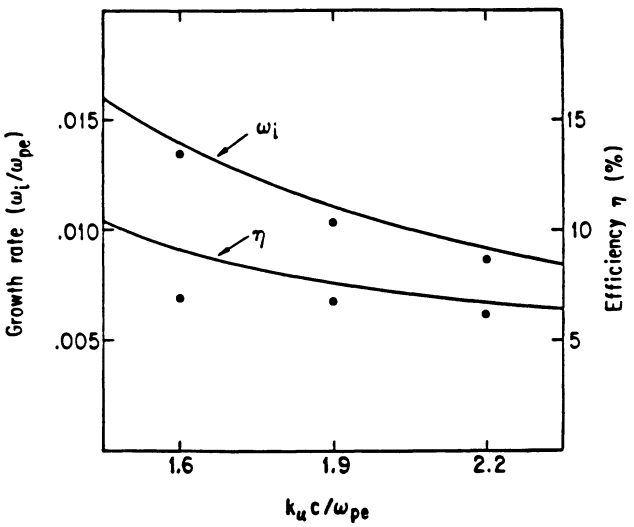

FIG. 4. Growth rate and efficiency from theory (solid lines) and simulation (discrete points) as a function of effective undulator wave number for the case of $\gamma=3$, $\theta=45°$, and $\epsilon_i=0.3$.

mate gives $\eta\sim 9\%$. The absolute instability of the forward scattered mode is observed to be responsible for this reduction. This instability can be decreased by increasing the effective wave number of the ion ripple and/or beam energy [8]. The efficiencies and growth rates of different $k_u c$ are given in Fig. 4 for the case of $\gamma=3$, $\epsilon_i=0.3$, and $\theta=45°$. As $k_u c$ increases, both efficiency and growth rate decrease. Note that the efficiency decreases slower than the growth rate. Figure 5 shows the dependence of efficiency and growth rate on beam energy for the case of $k_u c=1.6$, $\epsilon_i=0.3$, and $\theta=45°$. Both efficiency and growth rate decrease with increasing beam Lorentz factor. The decline of efficiency is faster than that of growth rate.

We will now compare the ion-ripple laser with FELs and ion-channel lasers (ICL) [10] and discuss the possible applications of the IRL. Because of technical limitations of undulator length (e.g., $\lambda_u > 1$ cm) and magnetic-field strength (e.g., $<5\times10^4$ G), conventional FEL requires a very-high-energy (e.g., $E\sim 1$ GeV) electron beam to produce short-wavelength (e.g., $\lambda\sim 10^3$ Å) radiation, but operates there with a low efficiency. This increases the electron-beam requirements, higher energy and higher current I; as well as magnet requirements, stronger and more uniform magnetic field and more precise undulator length and alignment. In addition, the gain and efficiency are small. Although some nonconventional FELs [11] can provide shorter undulators, the driving field is not steady or intense enough. ICL can have higher betatron oscillation frequency ($\omega_{pe}/\gamma^{1/2}$) and stronger driving force than conventional FELs, but the scaling of radiation frequency with the beam γ (i.e., $\omega\sim 2\gamma^{3/2}\omega_{pe}$) is something of a disadvantage.

By employing an IRL, the undulator length of ion ripple, λ_{ir}, can be shorter (e.g., $k_u c > \omega_{pe}\sim 4\times10^{12}$ rad/sec for $n_0=4\times10^{15}$ cm^{-3}) and can easily be adjusted; the ion-ripple field is steady and very high (e.g., $|E_{ir}|\sim 0.2$ GV/m for $n_0=4\times10^{15}$ cm^{-3}, $k_{ir}c=2\omega_{pe}$, and $\epsilon_{ir}=0.4$), and there is no need for an external magnet system. Thus IRLs using a lower-energy beam can provide the same frequency wave source with higher efficiency than FELs; higher efficiency means a larger beam energy spread is allowed. Power supplies can be simpler and the heavy radiation shield required for very-high-energy beams can be eliminated. Alternatively an IRL using the same energy beam as an FEL can produce shorter-wavelength coher-

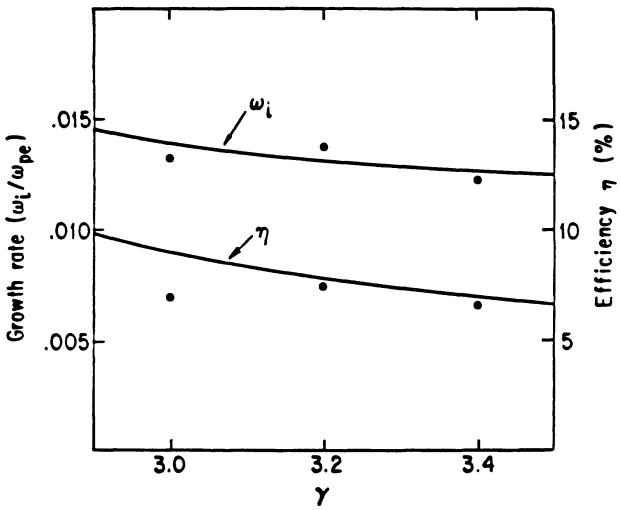

FIG. 5. Growth rate and efficiency from theory (solid lines) and simulation (discrete points) as a function of beam γ for the case of $k_u c/\omega_{pe}=1.6$, $\theta=45°$, and $\epsilon_i=0.3$.

TABLE I. Numerical examples of ion-ripple laser scalings.

	Microwave	Infrared	UV
E (MeV)	1	5	18
ΔE (keV)	<48	<34	<20
I (kA)	1	1	1
n_b (cm^{-3})	8.6×10^{9}	4.7×10^{13}	4.0×10^{15}
ϵ_n (πcm rad)	<0.86	$<4.4\times10^{-3}$	$<1.9\times10^{-4}$
λ_{ir} (cm)	13	0.17	0.019
λ (Å)	1×10^{8}	1×10^{5}	1×10^{3}
P (MW)	48	34	20

ent radiation.

Table I gives numerical examples of ion-ripple laser scaling in three frequency regimes for an electron beam with $\theta=45°$, and $k_u c\sim2\omega_{pe}$. The limitations on ΔE, the beam energy spread, and ϵ_n are given. The peak power of the radiation, P, is estimated by the backward Raman scattering scaling law. If the space-charge effects were not important, we would expect to obtain higher efficiency and higher output power. The effects of partial dielectric guiding of the radiation and ion-guiding of the electrons increase the overlap of the beam and radiation; tapering the ripple wavelength may also enhance lasing. Shorter wavelengths can be achieved by increasing the undulator wave number and/or the beam energy and by adjusting the angle of beam injection.

The scaling law given in this Letter is derived from the collective behavior of beam electrons. We note that, for a wavelength equal to or shorter than x rays, the electron spacing ($n_b^{-1/3}$) may be larger than the radiation wavelength. However, the linear density of a 1-kA beam is 2.1×10^{11} cm^{-1}; that is, there are more than 10^4 particles per wavelength (e.g., $\lambda\sim5$ Å) for an x-ray laser, which we assume to be a plane wave.

Although the lasing mechanism discussed in this Letter is applied to laboratory radiation sources with their very coherent beams and waves, the mechanism may also occur in nature and particularly in some astrophysical radiation sources.

In summary, we have proposed a new scheme to produce tunable laser sources from microwaves to the ultraviolet. With a simpler system and lower beam requirements, ion-ripple lasers can have higher frequency, efficiency, and output power than FELs as well as being more flexible. Analytic theory and PIC simulations were used to verify the concept and to study the mechanisms. To study more realistic situations, a 2 1/2 D simulation needs to be performed and experiments are recommended.

The authors would like to thank V. Decyk for helpful discussions on generating particle ripple distribution in the simulation code and S. Smith for his comments on the manuscript. This work is supported by the National Science Foundation, the Department of Energy, and the Lawrence Livermore National Laboratory.

[1] A. E. Dangor *et al.*, IEEE Trans. Plasma Sci. **15**, 161 (1987).
[2] See, for example, J. J. Su *et al.*, Phys. Rev. A **41**, 3321 (1990); W. E. Martin *et al.*, Phys. Rev. Lett. **54**, 685 (1985), and references therein.
[3] A. T. Lin *et al.*, Phys. Rev. A **8**, 2618 (1973); C. K. Birdsall, Proc. IRE **42**, 1628 (1954).
[4] K. R. Chen *et al.*, Phys. Fluids B **3**, 1270 (1991).
[5] T. Kwan *et al.*, Phys. Fluids **20**, 581 (1977).
[6] J. M. Dawson, Rev. Mod. Phys. **55**, 403 (1983); K. R. Chen and J. M. Dawson (to be published).
[7] H. Motz and M. Nakamura, Ann. Phys. (N.Y.) **7**, 84 (1959); L. R. Elias *et al.*, Phys. Rev. Lett. **36**, 717 (1976); C. W. Roberson and P. Sprangle, Phys. Fluids B **1**, 3 (1989), and references therein.
[8] P. C. Liewer *et al.*, Phys. Rev. A **23**, 1251 (1981).
[9] T. M. O'Neil and J. H. Malmberg, Phys. Fluids **11**, 1754 (1968).
[10] D. H. Whittum *et al.*, Phys. Rev. Lett. **64**, 2511 (1990); K. R. Chen *et al.*, IEEE Trans. Plasma Sci. **18**, 837 (1990).
[11] L. R. Elias, Phys. Rev. Lett. **42**, 977 (1979); G. Bekefi *et al.*, Phys. Rev. A **34**, 1228 (1986).